CHEMNANOMAT

CHEMISTRY OF NANOMATERIALS FOR ENERGY, BIOLOGY AND MORE

www.chemnanomat.org

Accepted Article

Title: Realizing Influence of Supports in Aqueous-Phase Hydrogenation of Furfural over Nickel Catalysts

Authors: Anil Singh Rajpurohit, Venkata Rama Mohan Talla, JACCOB MADHAVAN, Krishnamurthy Konda Ramaswamy, and Balasubramanian Viswanathan

To be cited as: *ChemNanoMat* **2023**, e202300158

Link to VoR: https://doi.org/10.1002/cnma.202300158

A Journal of

ACES Asian Chemical Editorial Society

WILEY VCH

Realizing Influence of Supports in Aqueous-Phase Hydrogenation of Furfural over Nickel Catalysts

Anil Singh Rajpurohit,[a,b] Talla Venkata Rama Mohan,[c] Madhavan Jaccob,*[a] Krishnamurthy Konda Ramaswamy*[b] and Balasubramanian Viswanathan*[b]

[a] Department of Chemistry & Loyola Institute of Frontier Energy (LIFE), Loyola College (Affiliated to University of Madras), Chennai-600034, India
E-mail: madhavanjack05@gmail.com
[b] National Centre for Catalysis Research, IIT Madras, Chennai-600036, India
E-mail: krkonda1949@gmail.com, bviswanathan@gmail.com
[c] Department of Chemistry, AdikaviNannaya University Campus-Tadepalligudem, Tadepalligudem -534101, India

Abstract

Catalytic activity of nickel nanoparticles (5% Ni w/w loading) dispersed on different metal oxide supports have been explored for the hydrogenation of furfural. Nickel, supported on reducible oxides (CeO_2 and TiO_2), display higher (almost 100%) conversion compared to that on non-reducible oxide supports (SiO_2, Al_2O_3, Mg_3AlO_x). H_2-TPR and XPS analyses bring out the influence of metal-support interaction during the reduction of nickel precursor and their electronic properties. The adsorption and activation of furfural on the catalyst has been studied using Infrared spectra and DFT calculations. The reaction proceeds via both ring-rearrangement and ring hydrogenation pathways, with furfuryl alcohol as the primary intermediate. At higher reaction temperature, reducible oxide supported catalysts, particularly titania, favours deep-hydrogenated products and higher conversion than non-reducible oxide supported catalysts. Among all the catalysts, nickel on titania displayed maximum conversion of furfural. TiO_2 possessing higher acidity than ceria, favoured ring-rearrangement of furfuryl alcohol to cyclopentanone at high temperatures, while the latter retarded reduction of cyclopentanone due to blockage of active-sites by unreacted furfural and strongly adsorbing intermediates. The combined effects of the electronic-state of supported metal and surface

acidity of catalyst provide a new strategy to tune catalytic properties for selective transformation during hydrogenation of furfural.

Introduction

Growing demands for energy and its dependence on declining fossil resources emphasizes the need for sustainable and renewable natural resources. Lignocellulose rich non-edible residues from agricultural crops have the potential to serve as a promising alternate feedstock for chemicals and fuels. Currently, most of the research on biomass is focused on its conversion to platform molecules through various conversion processes, such as, dehydration, hydrogenation, rearrangement, isomerisation, etc. Bio-derived chemicals, in comparison to petrochemicals, contain unsaturated bonds with high O/C ratio and small amounts of nitrogen, sulphur, phosphorous, etc., which provide reactive functionalities to a molecule.[1] This necessitates a clear understanding of these chemical transformations at atomic scale, to design functional materials that facilitate economically viable biomass valorisation processes.[2]

Recent studies have identified furan derivatives such as furfural, 5-hydroxymethyfurfural and 2,5-furandicarboxylic acid as sustainable platform molecules for chemical industry.[3] Among them, furfural (FAL) obtained via dehydration of xylose, on hydrogenation gives variety of value-added chemicals.[4] For example, furfuryl alcohol (FOL), due to its versatile applications, accounts for most of the revenue derived from furfural.[5] FOL is used for production of resins to bind foundry sand, laminating fibreglass reinforced equipment, corrosion resistance mortar, adhesive-hypergolic propellant, chemical intermediate for ranitidine, etc.,[6] Complete hydrogenation of furfural produces water miscible tetrahydrofurfuryl alcohol (THFOL). It is considered as a green solvent for use in inkjet inks, diluent for epoxy resins, paint stripper, flux remover and intermediate for polymers.

Cyclopentanone (CPO) and cyclopentanol (CPOL) are the rearrangement and deep hydrogenation products of furfuryl alcohol, used in the production of fragrances, flavouring agents, aviation fuels, polymer intermediates, drugs, agrochemicals, etc.,[7]. Therefore, selective saturation of bonds and intra-molecular rearrangements are the important aspects of a hydrogenation catalyst to achieve desired products.

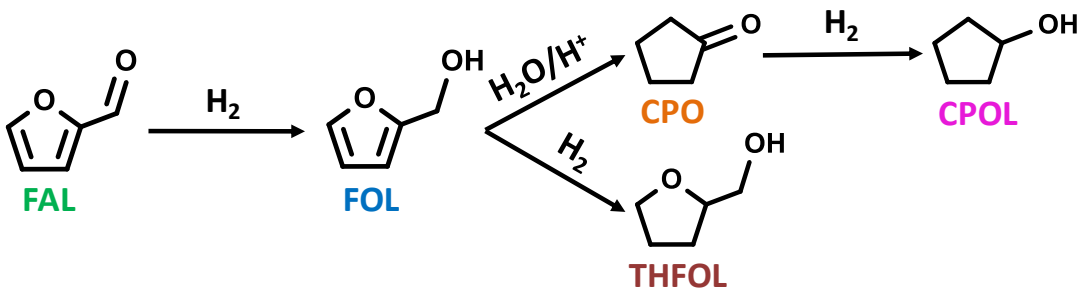

Scheme 1. Plausible pathways for catalytic hydrogenation of furfural in aqueous medium. [FAL =furfural; FOL = furfuryl alcohol; CPO = cyclopentanone; THFOL=tetrahydrofurfuryl alcohol; CPOL = cyclopentanol]

Supported metal catalysts have been studied extensively for the transformations of various organic compounds.[8] The activity and selectivity of these catalysts, especially on metal-oxide supports, are influenced by nature of the metal, metal dispersion, and metal-support interaction.[9] Increased awareness of biomass utilization has resulted in keen interest in development of tailored catalysts to tune product selectivity in furfural hydrogenation process. Commercially used Cu-Cr catalysts are to be replaced as chromium has adverse effects on environment.[10] Studies of furfural hydrogenation on NiO and, TiO_2 supports using Pd and Ir as catalysts showed that the product selectivity was directed by dual site mechanism giving emphasis for the metal-support interaction and interfaces.[11] Pt/γ-Al_2O_3catalysts specifically favoured C=O hydrogenation whereas Pd/γ-Al_2O_3 produced ring hydrogenated products[12]. Upon dispersion of Pt on sulphated zirconia, the acidic sites promoted

hydrogenolysis of furfuryl alcohol to form 2-methylfuran. Also, it was shown that the cooperative functionality of reaction sites at interface of Pt on hydrotalcite catalysts lead to ring opening of furfuryl alcohol intermediate by C-O scission, resulting in the formation of 1,2-pentanediol via 1-hydroxy-2-pentanone intermediate. Besides hydrogenation and ring-opening products, Hronec et al. reported ring-rearrangement process, by which furfural in aqueous medium transforms to cyclopentanone.[13]

Non-noble metal catalysts were also studied for the hydrogenation of furfural. For example, Arundhathi et al. have reported the higher activity of Cu impregnated on various supports, like, SiO_2, CeO_2, TiO_2, Al_2O_3 and MoO_3. It was shown that the selectivity towards furfuryl alcohol further increased by doping magnesium onto the support. However, deep hydrogenated products were not formed in this case.[14] Yang et al. detected 4-hydroxy-2-cyclopentenone as an intermediate during rearrangement reaction over Ni-Cu/SBA-15 catalyst, which on further hydrogenation formed cyclopentanone with 62 % yield.[15] With highly acidic HY zeolite supported Ni catalyst, 79% yield of rearrangement products could be achieved after 9h reaction time.[16] Ni/SiC catalyst, with no acidic sites, promoted ring rearrangement after adding metal salts (Lewis sites) or acid resins (Brönsted sites) externally to the aqueous solution of furfural. Similarly, presence of both these type of acidic sites on oxide surface can influence product selectivity.[17] The addition of Pd to Ni/TiO_2-ZrO_2 changes selectivity of the hydrogenation product from furfuryl alcohol to tetrahydrofurfuryl alcohol. Similarly, presence of alkaline earth metals in alumina supported Ni catalyst favoured ring hydrogenation over ring rearrangement reaction.[18] The improved selectivity towards furfuryl alcohol on addition of MgO to Cu/Al_2O_3 catalyst is attributed to synergistic effect of Cu-Mg species formed on the surface of alumina.[14] 5-Hydroxymethylfurfural, an analogue of furfural, undergo ring opening to 1,2,6-hexanetriol over Ni-Co-Al mixed oxides

catalysts, whereas Ni-Al catalyst lead to ring hydrogenated products, indicating synergistic effect between Ni and Co.[19]

Also, it was observed that reducible supports can impart dual functionality, as the surface with oxygen vacancies can also anchor the reacting molecule, thereby altering the selectivity. Baker et al. suggested that unsaturated aldehydes adsorb at the oxygen vacant sites of reducible support and selectively get hydrogenated to form alcohol by charge transfer from reduced support to the formyl group.[20] In presence of surface vacant sites, Au/CeO_2 catalyst in gas phase switches product selectivity from furfuryl alcohol to 2-methylfuran with increase in the reaction temperature of furfural. DFT studies on Ni/CeO_2 catalyst suggested that Ni cluster, in direct contact with surface oxygen vacancies, gains electron charge density. In the absence of Ni, the excess charge density partially occupies 4f orbitals of nearest Ce ions. Such charge transfer interaction between metal-support is also found in Ni/TiO_2 catalyst.[21] Ni et al. observed charge transfer from oxygen deficient ZrO_{2-x} to Ni, which accelerated liquid phase fatty acid hydrogenation towards alcohol production. Also, difference in metal oxide interactions with their supported metal is inferred to induce surface functionalities and reducibility behaviour.[22] This can alter electronic properties of metal and also provide additional reactive sites.

All these results suggest that the metal support interactions and the nature of support play a dominant role in the activity and selectivity for furfural hydrogenation. Also, to the best of our knowledge there are limited studies carried out on role of the metal-support interactions in nickel-based catalysts for furfural hydrogenation. Therefore, in this paper we investigated the role of the metal oxide supports in catalysing aqueous phase furfural hydrogenation over Ni catalysts.

The catalysts were prepared using nickel acetate as the precursor for nickel (5% w/w loading), using wet impregnation methods. Commercially available titania and silica supports were used as such whereas other supports (ceria, alumina and hydrotalcite) were synthesized. The detailed synthesis procedures for the support, the catalysts, and the characterization techniques used are given in the experimental section. The catalysts synthesized using silica, alumina, titania, ceria and hydrotalcite were designated as Ni/SiO_2, Ni/Al_2O_3, Ni/TiO_2, Ni/CeO_2 and, Ni/Hd, respectively. All these supported catalysts were reduced at 450^{o}C for 6 hours under hydrogen flow, thoroughly characterized and tested for furfural hydrogenation.

Results and Discussion

a. X-ray diffraction

X-ray diffractograms in Figure 1 display the phases and crystalline nature of the reduced Ni catalysts over different supports. Among different metal oxides, TiO_2 and CeO_2 show sharp peaks. The diffraction patterns of TiO_2 support shows peaks corresponding to both anatase and rutile phases that are indexed respectively using the JCPDS file numbers 21-1272 and 75-1753. The anatase to rutile phase composition ratio was found to be 77:23, in accordance with the literature. The titania phase composition was not altered during the calcination and reduction treatments used to impregnate nickel.[23] Similarly, CeO_2 showed fluorite type cubic crystal structure (JCPDS-81-0792) that was intact during the nickel impregnation process. SiO_2 (JCPDS-29-0085) and alumina (γ-Al_2O_3) (JCPDS-29-0063) supports exhibited amorphous nature with broad characteristic peaks that are retained even after nickel impregnation and reduction (Figure S1). On the other hand, in the case of hydrotalcite, we have observed a structural change on thermal treatment.

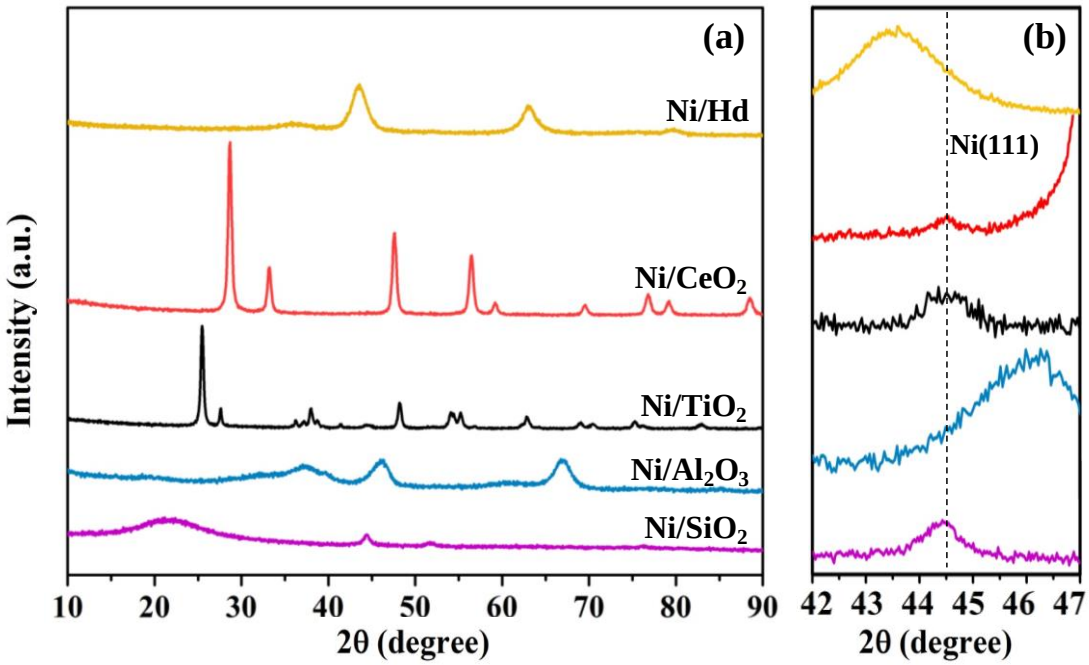

Figure 1. (a) XRD patterns of Ni catalysts supported over different metal oxides. (b) Enlarged portion of 2theta from 42°-47° to show the presence of metallic nickel.

Initially, the bare hydrotalcite phase exhibited Mg-Al double layer hydroxides structure (Figure S1). Upon nickel impregnation and subsequent calcination, it was transformed into mixed-metal oxide structure. The calcined sample has shown primarily the diffraction patterns of magnesia (JCPDS-01-1235) in which the alumina was dispersed and exist as binary oxide with magnesia.[24] Figure 1b shows the enlarged portion of the XRD patterns wherein the characteristics peaks of metallic Ni were clearly visible over TiO_2, CeO_2 and SiO_2 supports. The average crystallite sizes for (111) crystal planes of Ni, calculated using Scherrer equation are given in Table 1. However, on alumina and hydrotalcite catalysts, the peaks corresponding to metallic Ni or NiO could not be detected due to overlapping by the peaks with that of support. It is to be noted that the catalysts were calcined for longer time (6 h) to ensure complete thermal decomposition of nickel acetate, followed by reduction.[25] This is confirmed by FTIR spectra (see Figure S2), wherein after calcinations the symmetric and asymmetric stretching vibrations of carboxylate group *ca.* 1430 and 1560 cm^{-1} completely disappeared. The total nickel loading on the final catalyst probed using AAS, showed 4.5-5.0

wt% of nickel in all the catalysts (Table 1). This observation, combined with the XRD results confirms that the nickel was impregnated and reduced successfully over the various supports used in the present study.

b. Electron microscopy

The catalysts were further characterized using various imaging techniques, such as, SEM, TEM and elemental mapping. Figure S3 shows the SEM images used to find the differences in the morphology of as-prepared Ni catalysts. The micrograph of silica supported catalyst shows aggregation of small nanoparticles, whereas, the plates like non-uniform structures with rough surfaces were observed in the case of alumina-based catalyst. For ceria and titania supported catalysts, larger granular nanoparticles of 30-50 nm size have restrained agglomeration. The image of hydrotalcite supported catalyst exhibits large disordered flakes like morphology, which indicates that layers existed even after calcination/reduction process.[26] Elemental mapping (Figure S4) of all the catalysts shows uniform distribution of Ni over all oxide supports. Figure 2 displays the TEM images along with the corresponding histograms of the nickel particles. From the measured values as given in Table 1, it was found that the mean Ni nanoparticles sizes on silica and ceria supports were larger than those on other supports, revealing the role of metal-support interactions during the catalyst synthesis.

10.1002/cnma.202300158

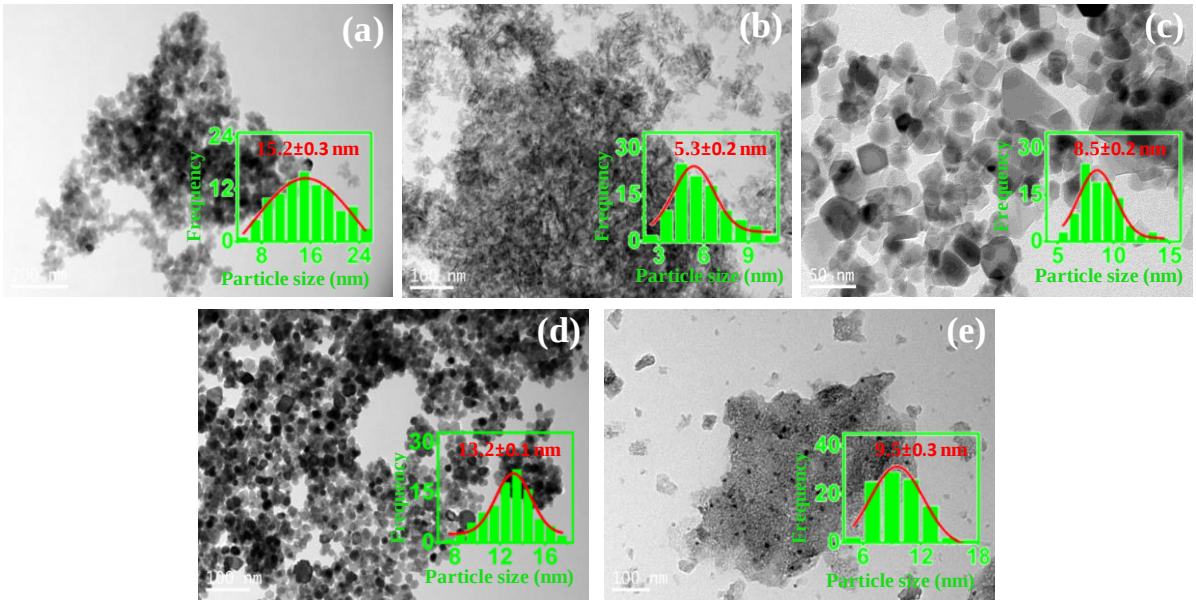

Figure 2. TEM images of Ni catalysts:(a) Ni/SiO_2, (b) Ni/Al_2O_3, (c) Ni/TiO_2, (d) Ni/CeO_2, (e) Ni/Hd. Inset shows particle size distribution.

c. Textural studies

Textural analysis results on all the catalysts are given in Figure S6 and Table S1. All catalysts showed type IV isotherms with H3 hysteresis, except for alumina supported catalyst that showed H1 hysteresis. The hydrotalcite derived catalyst showed highest BET surface area, followed by silica and alumina supported catalysts, showing almost similar surface area, which are then followed by titania and ceria, exhibiting very low surface area. However, when the surface analysis and imaging results were correlated, we see that the mere presence of higher surface area will not result in the smaller particle sizes of the impregnated metal. This is seen from hydrotalcite, alumina and silica supports that have similar surface area, with the first two giving rise to higher particle size (~ 9.5 nm for hydrotalcite and ~15.2 nm for silica supported), whereas alumina showing lower particle size (~5.3 nm). Also, for ceria and titania catalysts having similar surface areas, the former shows larger particle size whereas the latter shows smaller particle size. Therefore, it can be inferred that the dispersion of Ni does not merely depend on surface area but also on the surface functionalities of support such

as facets, functional groups, oxidation states, etc., effects the Ni precursor interaction with support, nucleation and growth of Ni nanoparticles.[27]

d. Surface acidity

Ammonia TPD results of Ni catalysts are summarized in Table 1, and desorption profiles are shown in Figure 3a. For all catalysts, a broad overlapped peaks profile, ranging within 190-511°C have been observed, suggesting the presence of acidic sites with different strength. Table S2 gives the peak positions of deconvolutions made for sites with different acidic strength. The weak acidic sites on all catalysts are found in desorption temperature range of 180-210°C, and medium strength sites between 230-350°C. Although the acidic sites found between 350-550°C are deconvoluted into two peaks, the strong acidic site strength is considered combining both the peaks. These high temperature desorption peaks are mainly observed for catalysts with high surface area. Both silica and alumina catalysts show nearly equal distributions of different acidic sites. The ammonia desorption from strong acidic sites on silica catalyst occurs at lower temperature than on alumina catalyst (Table S2). On the other hand, hydrotalcite derived catalyst showed that out of the total acidic sites, 64% were accounted for strong acidic sites with desorption temperature closer to alumina catalyst.

Table 1. Physico-chemical properties of supported Ni catalysts

Catalyst	Ni (wt%)[a]	D_{Ni} (nm) [b]	Ni Particle size (nm) [c]	Ni dispersion (%)[d]	Distribution of acidic sites (µmol/g) [e]				Density of acidic sites (µmol/m^2)[f]
					Weak	Medium	Strong	Total	
Ni/SiO_2	4.85	11.4	15.2	6.7	35	29	31	95	0.6
Ni/Al_2O_3	4.73	-	5.3	19.2	154	172	180	506	3.2
Ni/TiO_2	4.82	8.1	8.5	12.0	77	55	73	205	5.1
Ni/CeO_2	4.46	11.5	13.2	7.7	26	20	7	53	1.5
Ni/Hd	4.54	-	9.5	10.7	105	45	264	414	2.5

[a] Determined Ni loading from AAS measurements. [b] Calculated average crystallite size of Ni(111) using Scherrer equation. [c] Obtained from TEM. [d] Calculated using TEM particle size. [e] Measured from NH_3-TPD analysis. [f] (amount of acid sites)/(BET surface area)

In the case of ceria, the number of acidic sites decreases with temperature. It is interesting to see that the peak temperatures of strong acidic sites for titania and ceria catalysts are lower

compared to that of all other catalysts. On the other hand, the weak acid sites appeared at almost similar temperatures in all catalysts (Table S2). The total acidity is considerably higher for alumina-based catalyst, followed by hydrotalcite and titania supported. Silica supported catalyst, despite having high surface area, shows fewer total acid sites and ceria showing the least among all catalysts.

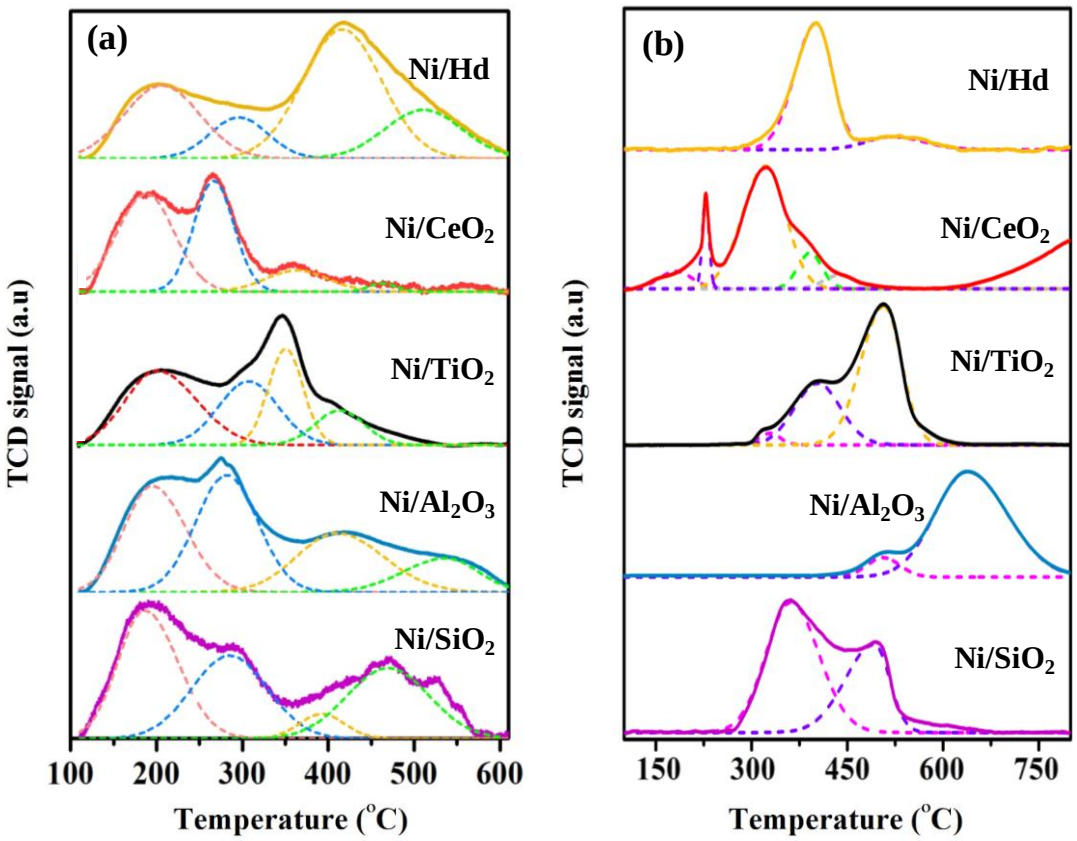

Figure 3. (a) NH_3-TPD and (b) H_2-TPR profiles of Ni catalysts supported on different metal oxides.

The density of acidic sites has been computed by normalising the total acid sites with the respective surface areas of catalyst. It is observed that the titania-based catalyst is having the highest density of acid sites followed by alumina, hydrotalcite, ceria and silica in that order. These results are in corroboration with the particle size distributions obtained from TEM analysis. For silica, alumina and hydrotalcite with similar surface area, the average Ni nanoparticle size decreases with increase in density of acid sites. The same observations are

valid for titania and ceria, where titania with higher acidic sites density is able to anchor smaller nanoparticles than on ceria.

e. Temperature programmed reduction

TPR profiles shown in Figure 3b reveal the interaction between Ni species and oxide supports, and its effect on the reduction behaviour of the catalysts. Ni/SiO_2 catalyst shows two reduction peaks at 362 and 490°C. The first peak is attributed to reduction of NiO nanoparticles weakly interacting with silica, while the second peak resulted from the reduction of NiO that is having strong interaction with SiO_2. However, it is worth mentioning here that Pantaleo et al. suggested formation of Si-O-Ni species, which is difficult to reduce. Also, He et al. reported that the NiO/SiO2 sample calcined at high temperatures requires higher reduction temperature suggesting increase in metal support interaction.[28] The reduction of NiO on alumina supported catalyst starts initially at 430°C. But most of reduction occurs above 500°C, suggesting better dispersion and therefore stronger interaction between NiO and support.[29] Ni/TiO_2 shows three reduction peaks at 322, 408 and 506°C. The reduction temperatures of Ni/TiO_2 catalyst are higher than that of Ni/SiO_2 catalyst, while Ni in Ni/CeO_2 is reduced at a lower temperature. The increase in reduction temperature for titania-based catalyst is due to the stronger interaction with support. On the other hand, the decrease in reduction temperatures on ceria supported catalyst is attributed to the reduction of adsorbed oxygen species on ceria oxygen vacancies, generated in the vicinity of Ni species which were incorporated into ceria lattice during impregnation and calcinations step.[30] These reduced sites facilitate the reduction of Ni species that are in direct contact with vacancies, giving a sharp peak at 228°C act as seed for further reduction of NiO at the lower temperature (321 and 390°C). Further, a small shoulder peak at 438°C can be ascribed to the reduction of ceria surface.[31] This surface change can lead to aggregation of small Ni nanoparticles reduced at lower temperatures resulting in a higher particle size as observed

from TEM particle size distribution.[32] Above 580°C, reduction of bulk ceria (inner region) occurs till that reaches maximum at 812°C. On Ni/Hd catalyst, a sharp peak at 399°C is attributed to the presence of NiO species interacting weakly with support, whereas the broad peak centred around 520°C is associated with the reduction of NiO that is strongly interacting with the magnesia-alumina binary oxide.[33]

f. X-ray photoelectron spectroscopy

XPS analysis has been used to study the chemical state of the elements and also demonstrate the interaction of metal with support. The binding energies of all samples are adjusted to 284.8 eV for C(1s). Figure 4 shows the nickel 2p core level XP spectra of the prepared catalysts post reduction. The Ni peaks are deconvulted in to $2p_{3/2}$, $2p_{1/2}$ and satellite peaks. As seen in Figure 4, all the catalysts show peaks corresponding to Ni^0 and Ni^{2+} $2p_{3/2}$ with binding energies located around 852.6 and 855.5 eV and Ni^0 and Ni^{2+} $2p_{1/2}$ with binding energies located around 869.0 and 873.0 eV.[34] As the reduced nickel catalysts were exposed to oxidation atmosphere in the interval between reduction and transfer to analysis chamber, the presence of Ni^{2+} peak in all the samples are imperative. From the spectra and the binding energy values given in Table S3, it is clear that the Ni^0 binding energy values decreased on the reducible supports. In the case of alumina catalyst, the peak at 854.3 eV is related to NiO reduction. Whereas, the peak at 857.9 eV is ascribed to the Ni^{2+} which is very close to the binding energy of Ni species observed in $NiAl_2O_4$ compound.[35] It correlates well with dispersion of small Ni nanoparticles observed from TEM, indicating strong interaction with alumina surface. Similar shift is observed for Ni species over silica catalyst, where Ni^{2+} shift to higher binding energy (856.5 eV) due to strong interfacial interaction.[36] On the other hand, hydrotalcite catalyst shows that most of the nickel is in metallic state that is attributed to the intercalation of Ni in the layered structure, which has protected it from re-oxidising during transfer of the catalyst for XPS analysis.[37]

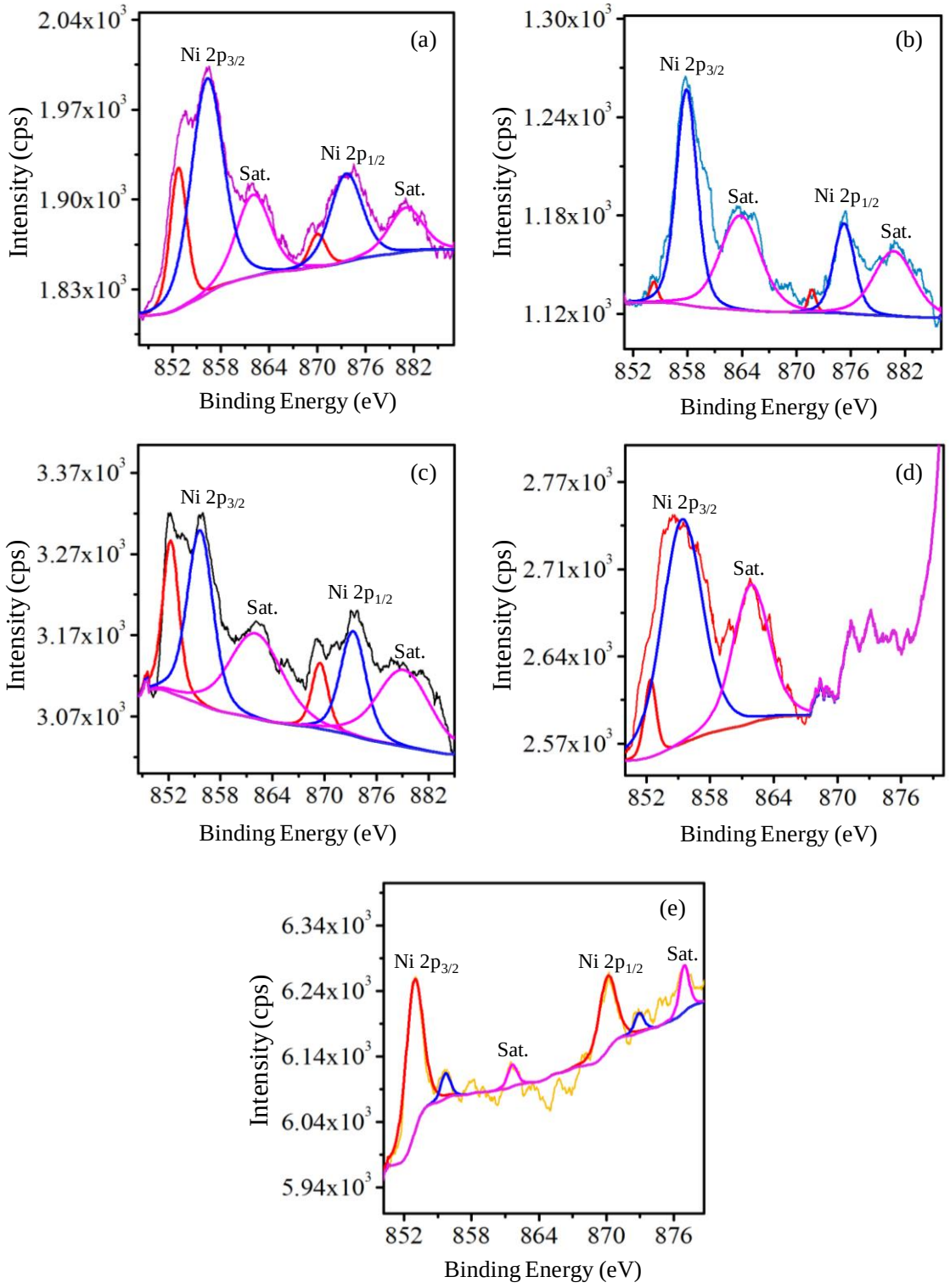

Figure 4. Core level Ni 2p XP spectra of (a) Ni/SiO_2, (b) Ni/Al_2O_3, (c) Ni/TiO_2, (d) Ni/CeO_2 and, (e) Ni/Hd catalysts.

From the Table S3 it is clear that the titania supported catalyst has higher Ni to support ratio among all the catalysts under study. Also, it is noteworthy that the Ni^0 peaks of

both titania supported and ceria supported catalysts are at similar binding energy.[21b,38] Therefore, to further probe, we have calculated the defective site ratios of both these supports, that are found to be, $\frac{Ti^{3+}}{(Ti^{3+}+Ti^{4+})} = 0.0522$, $\frac{Ce^{3+}}{(Ce^{3+}+Ce^{4+})} = 0.372$ (see Figure S6 for XPS core level spectra of the supports). These values suggest that, in ceria more defective sites are evolving on to the surface of the catalyst. This can result in a decrease in the amount of nickel that is present on the surface.[39] However, the lower dispersion of Ni at the surface of ceria than over titania can also contribute to the decrease in Ni to support ratio for ceria catalyst.[40] The deconvoluted spectra of all supports are shown in Figure S6. Silica support shows Si^{4+} peaks corresponding to amorphous form. On other hand, alumina peaks at 75.4 and 76.3 eV can be attributed to Al^{3+} in amorphous and crystalline γ-Al_2O_3. The Hd support shows Al^{3+} peak corresponding to AlO_x, whereas peaks at 52.5 and 54.8 eV of Mg^{2+} are assigned to Mg-OH and tetrahedral coordinated Mg^{2+} to oxygen in spinel like structure.

Figure S7 shows the O1s core level spectra of the prepared catalysts and all the samples have shown characteristic peaks of oxygen that are deconvoluted into multiple peaks associated with lattice oxygen, surface hydroxyl group and the adsorbed water or oxygen.[37,41b,42] The binding energy values corresponding to these peaks are given in Table S3. The O 1s binding energies for the reducible oxides (TiO_2 and CeO_2) and mixed metal oxide derived from hydrotalcite (Hd) are found at lower values compared with silica and alumina supports. The broad peak of ceria compared with titania is due to the presence of higher defective sites, as it is known that the introduction of Ni on ceria will promote the formation of oxygen defect sites.[42e,42f]

g. Catalytic activity for hydrogenation of furfural

i) Activity and selectivity patterns

All these well-characterized catalysts were then probed for the catalytic activity for hydrogenation of furfural (FAL) in aqueous medium. The reaction studies were carried out using Parr reactor and the products analysed using GC. The details of hydrogenation studies are given in the supporting information. The reactions were carried out at two different temperatures and the resultant product distribution values are given in Table S4 and in Figure 5. Under the given reaction conditions, furfural prefers either hydrogenation of C=C and/or C=O or ring rearrangement products. At 100°C reaction temperature, Ni/TiO_2 and Ni/CeO_2 showed 76.5%, and 64.0% conversion of FAL. All other catalysts showed a conversion less than 30%. However, it was seen that FOL was the predominant product in all the catalysts, suggesting that higher temperatures were required for further hydrogenation.

At 140°C reaction temperature, Ni/TiO_2 and Ni/CeO_2 showed 100% conversion followed by Ni/Al_2O_3, Ni/SiO_2 and Ni/Hd, showing conversions between 50-60%. In addition, the hydrogenation is not restricted to FOL, instead deep hydrogenated products are predominantly formed with varied selectivity towards different products via., tetrahydrofurfurylalcohol (THFOL), cyclopentanone (CPO), and cyclopentanol (CPOL). The selectivity towards CPO formation for Ni/SiO_2 was 75% and for Ni/Al_2O_3 was 73%, which was predominant over the formation of THFOL. It was also observed that on Ni/SiO_2 the THFOL selectivity decreased from 9% at 100°C to 4.8% at 140°C. On the other hand, in the case of Ni/Al_2O_3 catalyst, an increase in THFOL selectivity from 6% at 100°C to 8.9% at 140°C is seen. It is interesting to note that although both TiO_2 and CeO_2 supports have given similar conversions, there is a marked difference in their product selectivity. Interestingly among all the catalysts, only on Ni/TiO_2 FAL has undergone the hydrogenation considerably to form CPOL, although a significant amount of THFOL formation is also seen. On Ni/CeO_2 much of the FOL formed has not been hydrogenated further. Also, the amounts of THFOL

and CPO are formed with no preferential selectivity. The Ni/Hd has shown the least conversion with no deep hydrogenation or rearrangement products.

ii) Rationale behind the observed activity/selectivity patterns

The number of hydroxyl groups on silica are less that on alumina, this in turn will decrease the surface overlayer of metal ion precursor and thus prevents the metal support dispersion on silica catalyst. This has also resulted in the larger particle size of nickel on silica support compared with that of alumina support. The XRD results show no NiO peak in the case of silica catalyst (Figure 1). But in alumina catalyst due to overlap of diffraction from support and higher Ni dispersion, the presence of NiO cannot be ruled out. It is also evident from the H_2-TPR result that shows Ni reduction at higher temperature. However, the higher conversion of FAL on alumina catalyst than on silica catalyst suggests that the reduction of alumina catalyst for 6h in H_2 provides significant amount of reduced Ni sites for hydrogenation.

The presence of large size Ni nanoparticles on silica than on alumina catalyst can favour flat adsorption of FOL, which further hydrogenates to THFOL. However, this has not altered the selectivity of THFOL significantly (~3%) on silica catalyst at lower reaction temperature. Similar to silica and alumina catalysts, the hydrogenation of furfural over ceria and titania catalysts at 100°C also lead to the formation of THFOL along with FOL, where the larger Ni particles on ceria enhances THFOL selectivity by 2.9%. These results clearly suggest that the Ni particle size does not have much effect on product selectivity.

It is known that, once FOL formed it can further hydrogenate in two paths; (a) it can prefer acidic sites of support to undergo ring rearrangement to form CPO that further hydrogenates to give the end product CPOL or (b) ring hydrogenation of FOL resulting in formation of THFOL. The higher selectivity to FOL over all catalysts at lower reaction temperature is in line with DFT calculations that carried out using Ni cluster (shown in Figure S8). The result

shows that the weaker adsorption of FOL on Ni surface allows it to be replaced by FAL, which increases selectivity for FOL at the cost of decrease in selectivity for further hydrogenated product, THFOL. But at high temperature with the availability of alternate rearrangement route, FOL on silica catalyst prefer CPO formation. On other hand, on alumina catalyst, with the increase in FAL conversion, the THFOL formed (8.9 %) along with CPO.

The selectivity data on titania and ceria catalysts at 140°C shows that the catalysts favoured both ring rearrangement and ring hydrogenation of the formed FOL. Both catalysts showed similar selectivity (20%) towards the formation of THFOL. The amount of acidic sites calculated from the NH_3-TPD data, shows that mere presence of higher amount of acidic sites does not improve the selectivity towards ring rearrangement (CPO) products. The alumina catalyst has five times higher amount of acidic sites than silica catalyst, but showed nearly equal selectivity for CPO. On the other hand, the hydrotalcite derived catalyst also has significant amount of acidic sites higher than titania and ceria, but does not favour ring rearrangement. These results clearly suggest that the CPO selectivity mainly depends on the nature of the acidic sites rather than the amount of acidic sites. As reported earlier, the FOL rearrangement is initiated with protonation of alcohol, followed by C-O cleavage.[43] The intermediate carbocation ($C_5H_5O^+$) formed will then undergo Piancatelli rearrangement to cyclopentanone. In general, the basic oxides like ceria or hydrotalcite will remain protonated at pH 7 in aqueous medium as their point of zero charge will be at higher pH. At the initial stage of rearrangement reaction, it will be difficult for the positively charged protonated species formed from furfuryl alcohol by auto-ionization of water and subsequent carbocation intermediate to approach these positively charged surfaces. In other words, the strong protonation at the surface will neither allow furfuryl alcohol to protonate at surface nor will allow protonated FOL in water to interact with surface. This can be seen from their selectivity towards cyclopentanone. In comparison to ceria, this effect is more pronounced on

10.1002/cnma.202300158

hydrotalcite catalyst due to its much higher pH for point of zero charge. On other hand, the point of zero charge of titania lies at pH between 5 to 6, leads to maximum furfuryl alcohol rearrangement. The lower affinity of titania for protonation also helps furfuryl alcohol to initiate reaction at the surface by protonation. Similarly, the higher selectivity towards CPO over SiO_2 and Al_2O_3 based Ni catalysts suggest that the acidic sites readily protonate furfuryl alcohol to undergo ring-rearrangement reaction.[44]

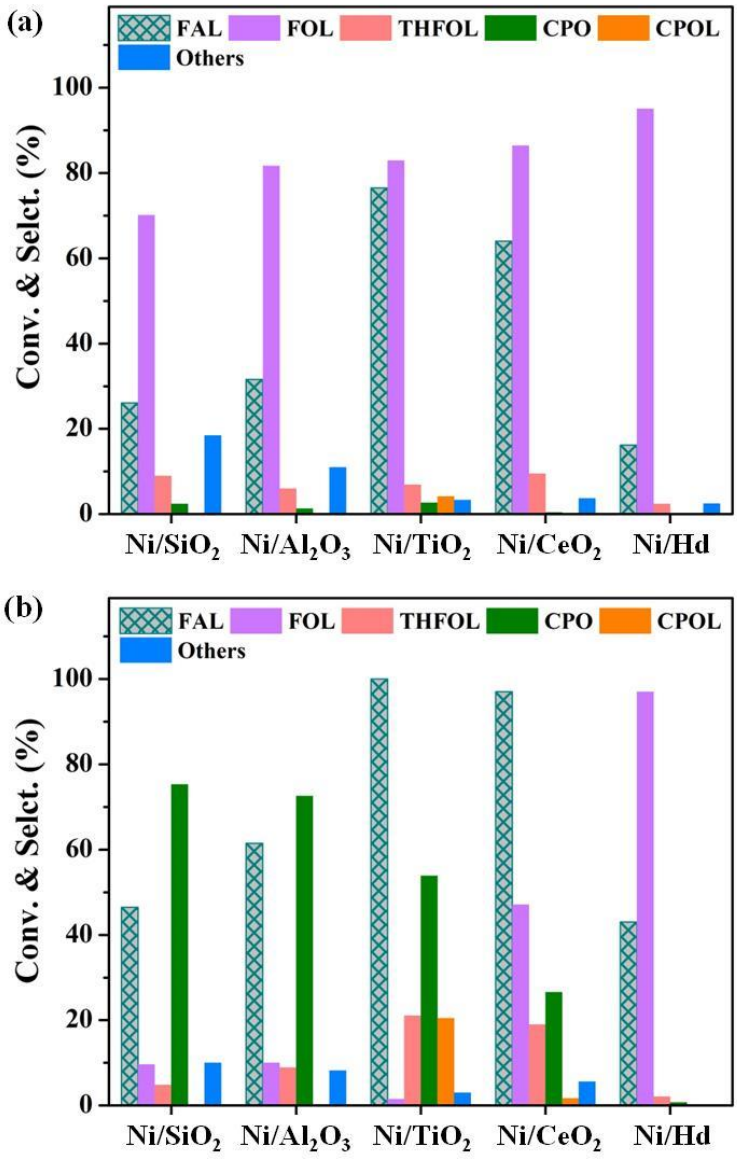

Figure 5. Conversion of Furfural and its products distribution at (a) 100°C and (b) 140°C.

Reaction conditions: 50 mL 5.2 mmol aqueous furfural solution, 100 mg catalyst, 5 MPa H_2, 4 h.FAL: furfural, FOL: furfuryl alcohol, THFOL: tetrahydrofurfuryl alcohol, CPO: cyclopentanone, CPOL: cyclopentanol.

In the case of double hydroxide layered structure, the hydrotalcite accommodate carbonate ions in between layers to counterbalance the charge imbalance caused by partial substitution (Mg/Al=3) of Al^{3+}. On impregnation, partially Ni^{2+} ions get intercalated between layers to interact with negatively charged carbonate ions. This additional intercalation increases d-spacing between (003) basal planes from 7.68 to 7.73 Å. The XRD results (Figure S1) showed decomposition of layer double hydroxide to mixed metal oxides on calcination. Also the lower H_2 consumption in TPR data and the low Ni/support ratio from the XPS data shows that some of the nickel is partially gone in between the layers of the support making it inaccessible for the reaction. This has resulted in the lower activity of the hydrotalcite based catalyst.

An additional catalyst with pure MgO support was also prepared by impregnation method (Figure S1 and S2). As shown in Figure S9, it gave 14% FAL conversion with 5% selectivity to FOL at 100ºC. This conversion increases to 23% at 140ºC with increase in FOL selectivity to 92.5%. These results suggest that the presence of alumina in hydrotalcite derived catalyst has significantly prevented the other side reactions.

iii) Reducible Vs Non-reducible supports

In comparison to non-reducible supports, the higher conversion for furfural obtained over ceria and titania catalysts suggests that the catalytic activity does not solely depend on metal dispersion. Instead, the support can provide more than one type of active site leading to different pathways/products. These support-based reactivity variations prompted us to look into the mode of substrate adsorption on catalyst surface. The FT-IR spectra in Figure 6 show characteristic carbonyl stretching vibration for pure furfural at 1642 cm^{-1}. Post adsorption, the spectra of the catalysts revealed that there is no significant shift in C=O stretching frequency (1637 and 1633 cm^{-1}), for silica and alumina catalysts. On the contrary, on titania and ceria

catalysts blue shifts to 1617 and 1593 cm^{-1} are seen. Combining these with the fact that there is no tetrahydrofurfuraldehyde formed in the reaction with any of the catalysts, suggests that in all the catalysts, the hydrogenation proceeds through carbonyl group. Similar observations were also reported by Baker et al., where on probing the titania surface using sum frequency generation (SFG) vibrational spectroscopy, they found the formation of alkoxy intermediate anchored on oxide via carbonyl oxygen.[20a] However, such species were not found on Pt/SiO_2. They have also performed DFT studies that revealed carbonyl activation involved charge transfer interaction at oxygen vacant site on support, which are in line with the observations made for crotonaldehyde.[20b] Also, in the present work XPS data showed reduction of both titania and ceria supports which provides further evidence for the presence of vacant sites on these supports for interacting with the carbonyl bond. Therefore, all the above observations imply that the enhancement of reaction on titania and ceria catalyst takes place through adsorption of aldehyde via oxygen lone pair on surface oxygen vacancies created during reduction process.

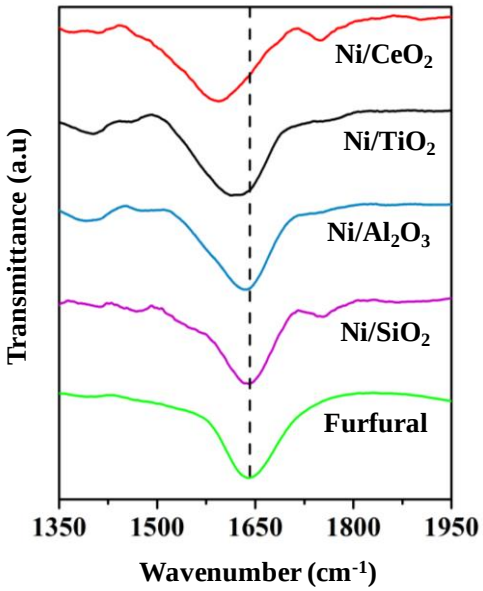

Figure 6. FT-IR spectra of pure furfural in pure form and after adsorption on different Ni catalysts.

Further to scrutinize the possibilities of carbonyl group activation and deep hydrogenated product selectivity, we predict that the availability of active metal site near to the adsorption site of alkoxide formation will favour the activation of carbonyl group and the further hydrogenation. In the studies by Baker and Kennedy although they found alkoxide formation on titania support, they also determined that the turnover of furfuryl alcohol or crotyl alcohol cannot be achieved without having direct contact between titania and Pt nanoparticles.[20] Yang et al., in his study of Pt-TiO_2 and Pt-CeO_2 system also emphasized the active role of accessible Pt surface near the support-metal interface and proposed that alkoxide formed at interface migrates to metal site for further hydrogenation.[45] In our case, the reaction is taking place under high hydrogen pressure and at an elevated temperature in liquid phase. These reaction conditions will favour the availability of dissociated hydrogen on Ni surface that in turn can react with interface species at vacant site for reaction. Therefore, activation of carbonyl group can occur at the interface region over titania and ceria catalysts.

Further hydrogenation of CPO to CPOL was observed only on titania catalyst. On all other catalysts the unreacted furfural would have blocked reactive sites. Li et al. studied formation of deep hydrogenated products on Pd/$NiMO_4$ catalysts. They have shown that large Pd nanoparticles were unable to hydrogenate cyclopentanone in presence of furfural or other intermediates.[46] Zhou et al. observed that the CPO hydrogenation did not proceed on 10 wt% Ni/CNT catalyst even after 10 h. They found CPOL product only at a very high Ni loading.[47] Our preliminary DFT studies have shown that the furfural and FOL adsorb stronger than CPO on Ni cluster, which can hinder cyclopentanone adsorption on catalyst for further reaction. Similarly, the interface sites can be blocked by unreacted furfural. On titania catalyst due to complete hydrogenation of furfural and furfuryl alcohol transformation, the active sites are therefore available for cyclopentanone reaction.

iv) Characterization of used catalysts and re-use

The characterization of the spent catalyst is also examined to access the stability of the prepared catalysts. In all the catalysts the Ni leaching is seen to be below 6 ppm after the reaction (Table S6) and is accompanied by an increase in the crystallite size as shown from the XRD patterns of the spent catalysts (see Figure S10). The FTIR spectra (in Figure S11a) obtained for all dried spent catalysts after reaction at 140°C shows presence of small amount of adsorbed furfural and/or products. The recyclability tests (Figure S12) were conducted over three cycles using ceria and titania catalysts. The catalyst was separated after every cycle and reused for next cycle. In case of ceria catalysts, the conversion decreases from 97% in first cycle to 81.9% in second cycle and then to 66.1% in third cycle. The FOL selectivity decreases slightly from 47.1 to 40.5%, whereas the CPO increases from 26.6 to 33.1%. The furfural conversion over titania catalyst remain almost stable during three recycles. The selectivity towards ring rearrangement on titania catalyst increases by ~5% with decrease in ring hydrogenation product, THFOL. The catalysts were characterized after three cycles and the resulting XRD and FT-IR are shown in Figure S11b and S13. The XRD pattern shows stable crystal structure of both catalysts. However, the FT-IR spectra have shown significant amount of intermediates/products adsorption on ceria than on titania catalyst, which has blocked active sites on ceria catalyst for reaction during recycling test. Overall, the reactions result shows that the both conversion and selectivity are retained on titania catalyst, suggesting it as a promising candidate for hydrogenation reaction.

In this work, the Ni/TiO_2 catalysts showed excellent catalytic activity than recently reported systems. Li et al. showed 100% FAL conversion with Ni loading of 20 wt% on anatase titania support. They have shown 51.2% selectivity for ring rearrangement. The selectivity was improved to 69.6% on replacing 50% Ni content with Co.[48] Recently, Chen et al. have synthesized Ni catalysts over P25 by reduction H_2 for 3h and suggested synergistic role of

formed Ni-NiO heterojunction on P25 for furfural hydrogenation.[49] However, in present this work, we have reduced calcined sample for longer interval of time to ensure complete reduction. Though XRD shows absence of NiO in titania catalyst, the role of small fraction of oxidised surface formed during transfer of sample cannot be discarded completely. Compare to the literature, even with lower Ni content our catalyst has exhibited higher catalytic activity. The Ru nanoparticle interaction with TiO_x on anatase titania support and addition of Co can enhance catalytic activity for FAL hydrogenation to FOL.[50] Hence, we can say that all the factors such as support, amount of active metal sites, the availability of defect site near to the metal-support interface, and the reaction temperature will have an influence on the activity, and selectivity of the hydrogenation of furfural.

Conclusion

Herein, the results show a synergistic effect between metal oxide support and Ni nanoparticles that determine the product selectivity for furfural hydrogenation. Ni nanoparticles supported over reducible oxides have significantly enhanced the catalytic activity in aqueous medium. Better availability of active sites near to the defective oxygen vacancies, the metal support interaction, the availability of dissociated H_2 make the nickel impregnated titania catalysts a suitable candidate for deep furfural hydrogenation. The acidity of catalyst along with water activates the bifunctional route for cyclopenatnone/cyclopentanol production at high temperature. The oxides support either with smaller number of acidic sites and/or point of zero charge of surface at higher pH resulted in incomplete transformation of furfuryl alcohol. Such surfaces will interact weakly with positively charged intermediates during rearrangement process. Our DFT calculations suggested that furfural and furfuryl alcohol in reaction medium regulate cyclopentanone hydrogenation. Titania supported catalyst has shown optimum catalytic activity towards furfural hydrogenation. Its active bifunctional sites have led to complete rearrangement of furfuryl alcohol to cyclopentanone

and further hydrogenation to cyclopentanol. Our work demonstrates the influence of support and strategies to catalyse selective hydrogenation and further acid catalysed rearrangements and deep hydrogenation processes for up-grading furan-based biomass chemicals. In addition, these active Ni based catalytic processes can pave the way to balance catalyst efficiency and the cost for commercial use.

Experimental Section

Synthesis of Ni catalysts: Ni catalysts on different supports (P25, SiO_2, CeO_2, γ-Al_2O_3, Hd and MgO) were prepared by wetness impregnation method. In brief, 0.64 g (equal to 5 wt%) of $Ni(CH_3COO)_2.4H_2O$ was dissolved in 30 mL of deionized water, followed by the addition of 2.85 g support (except Hd) with continuous stirring at 60 ^oC. Water was then evaporated slowly at 60 ^oC and further dried at 100 ^oC overnight in air oven. The dried sample was calcined at 450 ^oC for 6 h in air (heating rate of 5 ^oC/min). Subsequently all samples were treated in the hydrogen flow at 450 ^oC for 6 h (heating rate of 5 ^oC/min). Similarly, the catalyst derived from hydrotalcite was prepared by adding 5.08 g dried Hd support (equals to 2.85 g Mg_3AlO_x after calcination) to 7 mL $Ni(CH_3COO)_2.4H_2O$ (0.64 g) aqueous solution. The sample was dried in air at 60 ^oC and then at 100 ^oC overnight. It was then calcined at 450 ^oC for 6 h in air, followed by reduction at 600^oC for 6 h (heating rate of 5 ^oC/min). The metal loading was maintained at 5 wt % on all supports.

Supporting Information

The manuscript includes a supporting information file. Supports preparations, experimental procedure, characterization details, reactions, DFT figures and coordinates are provided in the supplementary file.[48-55] The supplementary information also includes figures and tables.

Conflict of Interest

The authors declare no conflict of interest.

Acknowledgements

The authors are grateful to the Department of Science and Technology (DST), New Delhi, for funding National Centre for Catalysis Research, IIT-Madras. The authors would like to thank Prof. G. V. Shanbag, Poornaprajna Institute of Scientific Research, Bengaluru, for help with the TPD and TPR instrument. We acknowledge Nanotechnology Research Centre (NRC), SRMIST for providing the research facilities.

Keywords: Furfural • Hydrogenation • Ring-rearrangement • Nickel • Oxides • Supported catalysts • Metal-support interaction

References

[1] U. K. Bhui, S. K. Pal, in *Macromolecular Characterization of Hydrocarbons for Sustainable Future. Green Energy and Technology* (Ed.: U. K. Bhui), Springer, Singapore, **2021**, Ch. 2, pp. 19-32.

[2] D. J. C. Constable, M. Gonzalez, S. A. Morton, in *Sustainability in the Design, Synthesis and Analysis of Chemical Engineering Processes* (Eds.: G. R. Mercado, H. Cabezas, Butterworth-Heinemann, Oxford, **2016**, Ch. 3, pp. 1-34.

[3] a) Top Value Added Chemicals from Biomass, Vol. 1 (Ed.: T. Werpy, G. Petersen), Office of Scientific and Technical Information (OSTI), Oak Ridge, TN, USA, **2004**, Vol. 1; b) J. J.Bozell, G. R. Petersen, *Green Chem.* **2010**, *12(4)*. 539-554.

[4] a) A. Jaswal, P. P. Singh, T. Mondal, *Green Chem.* **2022**, *24*, 510-551; b) N. W. Dulie, B. Woldeyes, H. D. Demsash, A. S. Jabasingh, *Waste Biomass Valor*. **2021**, *12*, 531–552.

[5] G. Gómez Millán, R. P. Bangalore Ashok, P. Oinas, J. Llorca, H. Sixta, *Biomass Convers. Biorefin.* **2021**, *11(5)*, 2095–2106.

[6] a) C. R. Schmitt, *Polym. Plast. Technol. Eng.* **1974**, *3(2)*, 121–158; b) G. Carotenuto, L. Nicolais, *Adv. Compos. Lett.* **1998**, *7(4)*, 105-109; c) M. V. K. Bhosale, S. G. Kulkarni, P. S. Kulkarni, *ChemistrySelect* **2016**, *1(9)*, 1921–1925; d) M. Mascal, S. Dutta, *Green Chem.* **2011**, *13(11)*, 3101–3102; e) X. Xi, Z. Wu, A. Pizzi, C. Gerardin, H. Lei, G. Du, *J. Adhes.* **2020**, *96(9)*, 814–838.

[7] a) K. J. Barnett, D. J. McClelland, G. W. Huber, *ACS Sustain. Chem. Eng.* **2017**, *5(11)*, 10223–10230; b) A. Corma, S. Iborra, M. Mifsud, M. Renz, M. Susarte, *Adv. Synth. Catal.* **2004**, *346(2–3)*, 257–262; c)P. Mäki-Arvela, N. Shcherban, C. Lozachmeur, K. Eränen, A. Aho, A. Smeds, N. Kumar, J. Peltonen, M. Peurla, V.

Russo, K. P. Volcho, D. Y. Murzin, *Catal. Lett.* **2019**, *149(5)*, 1383–1395; d) J. Scognamiglio, L. Jones, C. S. Letizia, A. M. Api, *Food Chem.Toxicol.* **2012**, *50(3)*, S608-S612; e) X. Sheng, N. Li, G. Li, W. Wang, J. Yang, Y. Cong, A. Wang, X. Wang, T. Zhang, *Sci. Rep.* **2015**, *5*, 9565; f) E. M. Samir, *OALib* **2016**, *3*, 1–11; g) D. Lisicki, B. Orlińska, *Polish J. Chem. Technol.* **2018**, *20(4)*, 102–107; h) S. Dutta, N. S. Bhat, *ACS Omega*, **2021**, *6(51)*, 35145–35172.

[8] a) L. Liu, A. Corma, *Chem. Rev*. **2018**, *118*, 4981–5079; b) M. J. Ndolomingo, N. Bingwa, R. Meijboom, *J. Mater. Sci*. **2020**, *55*, 6195–6241.

[9] a) R. Mistri, B. Kumar, *Asian J. Chem*. **2021**, *33(3)*, 489–498; b) I. Ro, J. Resasco, P. Christopher, *ACS Catal*, **2018**, *8(8)*, 7368–7387.

[10] K. Yan, A. Chen, *Energy* **2013**, *58*, 357–363.

[11] a) S. Campisi, C. E. C. Thaw, L. E. Chinchilla, A. Chutia, G. A. Botton, K. M. Mohammed, N. Dimitratos, P. P. Wells, A. Villa, *ACS Catal.* **2020**, *10*, 5483-5492; b) S. Campisi, D. Motta, I. Barlocco, R. Stones, T. W. Chamberlain, A. Chutia, N. Dimitratos, A. Villa, *ChemCatChem* **2022**, *14(6)*, e202101700.

[12] S. Bhogeswararao, D. Srinivas, *J. Catal.* **2015**, *327*, 65–77.

[13] a) T. Mizugaki, T. Yamakawa, Y. Nagatsu, Z. Maeno, T. Mitsudome, K. Jitsukawa, K. Kaneda, *ACS Sustain. Chem. Eng.* **2014**, *2(10)*, 2243–2247; b) M. Hronec, K. Fulajtarová, *Catal.Commun.* **2012**, *24*, 100–104.

[14] R. Arundhathi, P. L. Reddy, C. Samanta, B. L. Newalkar, *RSC Adv.* **2020**, *10(67)*, 41120–41126.

[15] Y. Yang, Z. Du, Y. Huang, F. Lu, F. Wang, J. Gao, J. Xu, *Green Chem.* **2013**, *15(7)*, 1932–1940.

[16] C. Y. Liu, R. P. Wei, G. L. Geng, M. H. Zhou, L. J. Gao, G. M. Xiao, *Fuel Process. Technol.* **2015**, *134*, 168–174.

[17] a) Z. Yu, H. Tian, K. Sun, Y. Shao, L. Zhang, S. Zhang, P. Duan, Q. Liu, S. Niu, D. Dong, X. Hu, *Mol. Catal.* **2020**, *496*, 111187; b) N. S. Date, S. E. Kondawar, R. C. Chikate, C. V. Rode, *ACS Omega* **2018**, *3(8)*, 9860–9871.

[18] a) B. Chen, F. Li, Z. Huang, G. Yuan, *Appl. Catal. A: Gen.* **2015**, *500*, 23-29; b) Y. Yang, J. Ma, X. Jia, Z. Du, Y. Duan, J. Xu, *RSC Adv.* **2016**, *6*, 51221-51228.

[19] S. Yao, X. Wang, Y. Jiang, F. Wu, X. Chen, X. Mu, *ACS Sustain. Chem. Eng.* **2014**, *2*, 173–180.

[20] a) L. R. Baker, G. Kennedy, M. van Spronsen, A. Hervier, X. Cai, S. Chen, L. W. Wang, G. A. Somorjai, *J. Am. Chem. Soc.* **2012**, *134(34)*, 14208–14216; b) G. Kennedy, L. R. Baker, G. A. Somorjai, *Angew. Chem. Int. Ed.* **2014**, *53(13)*, 3405–3408.

[21] a) M. Li, L. Collado, F. Cárdenas-Lizana, M. A. Keane, *Catal. Lett.* **2018**, *148(1)*, 90–96; b) K. R. Hahn, A. P. Seitsonen, M. Iannuzzi, J. Hutter, *ChemCatChem* **2015**, *7(4)*, 625–634; c) M. Xu, S. He, H. Chen, G. Cui, L. Zheng, B. Wang, M. Wei, *ACS Catal.* **2017**, *7(11)*, 7600–7609; d) X. Zhang, P. Yan, B. Zhao, Z. C. Zhang, *Catal. Sci. Technol.* **2021**, *11(1)*, 297–311.

[22] a) J. Ni, W. Leng, J. Mao, J. Wang, J. Lin, D. Jiang, X. Li, *Appl. Catal. B* **2019**, *253*, 170–178; b) X. Zhang, P. Yan, B. Zhao, K. Liu, M. C. Kung, H. H. Kung, S. Chen, Z.

C. Zhang, *ACS Catal.* **2019**, *9(4)*, 3551–3563; c) W. She, T. Qi, M. Cui, P. Yan, S. W. Ng, W. Li, G. Li, *ACS Appl. Mater. Interfaces.* **2018**, *10*, 14698–14707; d) L. Tan, T. Li, J. Zhou, H. Chen, F. Jiang, *Colloids Surf. A: Physicochem. Eng. Asp.* **2018**, *558*, 211-218.

[23] R. A. Spurr, H. Myers, *Anal. Chem.* **1957**, *29(5)*, 760-762.

[24] D. Wierzbicki, R. Baran, R. Dębek, M. Motak, T. Grzybek, M. E. Gálvez, P. da Costa, *Int. J. Hydrogen Energy* **2017**, *42(37)*, 23548–23555.

[25] J.C. de Jesus, I. González, A. Quevedo, T. Puerta, *J. Mol. Catal. A: Chem.* **2005**, *228*, 283–291.

[26] P. Hájková, Z. Tišler, *Catal. Lett.* **2017**, *147(2)*, 374–382.

[27] a) Y. Sun, H. Wang, P. Li, H. Geng, J. Xu, Y. Han, *Eur J. Inorg. Chem.* **2018**, *2018(16)*, 1715–1725; b) L. R. Borges, A. G. M. da Silva, A. H. Braga, L. M. Rossi, M. A. Suller Garcia, P. Vidinha, *ChemCatChem* **2021**, *13(5)*, 1340–1354; c) Y. Zhou, L. Du, Y. Zou, J. Zhou, *Surf. Sci.* **2019**, *681*, 47-53; d) G. Zhou, L. Jiang, D. He, *J. Catal.* **2019**, *369*, 352–362.

[28] a) H. D. Setiabudi, K. H. Lim, N. Ainirazali, S. Y. Chin, N. H. N. Kamarudin, *J. Mater. Environ. Sci.* **2017**, *8(2)*, 573–581; b) B. Zhao, Z. Chen, X. Yan, X. Ma, Q. Hao, *Top. Catal.* **2017**, *60(12–14)*, 879–889; c.) G. Pantaleo, V. L. Parlo, M. L. Testa, A. M. Venezia, *Ind. Eng. Chem. Res.* **2021**, *60*, 18684-18694; d.) S. He, X. Zheng, L. Mo, W. Yu, H. Wang, Y. Luo, *Mater. Res. Bull.* **2014**, *49*, 108-113.

[29] L. Zhou, L. Li, N. Wei, J. Li, J. M. Basset, *ChemCatChem* **2015**, *7(16)*, 2508–2516.

[30] L. Wang, Y. Liu, *Chem. Lett.* **2008**, *37(1)*, 74–75.

[31] a) Z. Tang, H. Cao, Y. Tao, H. J. Heeres, P. P. Pescarmona, *Appl. Catal. B* **2020**, *263*. 118273; b) X. Huang, J. Li, J. Wang, Z. Li, J. Xu, J. *Front. Chem. Sci. Eng.* **2020**, *14(4)*, 534–545.

[32] Y. Zhou, J. M. Perket, A. B. Crooks, J. Zhou, *J. Phys. Chem. Lett.* **2010**, *1(9)*, 1447-1453.

[33] C. Miao, F. Wang, G. Zhou, H. Xie, Z. Jiao, X. Zhang, *Int. J. Chem. React. Eng.* **2019**, *17(12)*. 20190006.

[34] a) J. Zhang, Y. Wang, C. Zhang, H. Gao, L. Lv, L. Han, Z. Zhang, *ACS Sustain. Chem. Eng.* **2018**, *6(2)*, 2231–2239; b) J. Wang, Q. Zhao, H. Hou, Y. Wu, W. Yu, X. Ji, L. Shao, *RSC Adv.* **2017**, *7*, 14152–14158.

[35] a) L. He, Y. Ren, B. Yue, S. C. E. Tsang, H. He, *Processes* **2021**, *9(4)*, 706; b) G. Garbarino, P. Kowalik, P. Riani, K. Antoniak-Jurak, P. Pieta, A. Lewalska-Graczyk, W. Lisowski, R. Nowakowski, G. Busca, I. S. Pieta, *Ind. Eng. Chem. Res.* **2021**, *60(18)*, 6554–6564.

[36] a) Z. Li, L. Mo, Y. Kathiraser, S. Kawi, *ACS Catal.* **2014**, *4(5)*, 1526–1536, b) B. Mallesham, P. Sudarsanam, B. Venkata Shiva Reddy, B. Govinda Rao, B. M. Reddy, *ACS Omega* **2018**, *3(12)*, 16839–16849, c) P. Weerachawanasak, P. Krawmanee, W. Inkamhaeng, F. J. Cadete, S. Aires, T. Sooknoi, J. Panpranot, *Catal. Commun.* **2021**, *149*, 106221.

[37] M. Zhang, F. Yu, J. Li, K. Chen, Y. Yao, P. Li, M. Zhu, Y. Shi, Q. Wang, X. Guo, *Catalysts* **2018**, *8*, 363.

[38] a) B. Cui, H. Wang, J. Han, Q. Ge, X. Zhu, *J. Catal.* **2022**, *413*, 880–890; b) J. Kaung, Z. Xing, J. Yin, Z. Li, S. Tan, M. Li, J. Jiang, Q. Zhu, W. Zhou, *Arab. J. Chem.* **2020**, *13*, 2568-2578; c) S. B. Kim. A. A. S. Eissa, M. J. Kim, E. S. Goda, J. R. Youn, K. Lee, *Catalysts* **2022**, *12*, 423.

[39] a) A. Cárdenas-Arenas, A. Quindimil, A. Davó-Quiñonero, E. Bailón-García, D. Lozano-Castelló, U. De-La-Torre, B. Pereda-Ayo, J. A. González-Marcos, J. R. González-Velasco, A. Bueno-López, *Appl. Mater. Today* **2020**, *19*, 100591; b) A. Caballero, J. P. Holgado, V. M. Gonzalez-Delacruz, S. E. Habas, T. Herranz, M. Salmeron, *Chem. Commun.* **2010**, *46(7)*, 1097–1099.

[40] N. S. Resende, C. A. Perez, J. G. Eon, M. Schmal, *Catal Lett.* **2011**, *141(11)*, 1685-1692.

[41] a) P. Post, L. Wurlitzer, W. M. Friedrichs, A. P. Weber, *Nanomaterials* **2018**, *8*, 530; b) Q. Liu, H. Qin, J. A. Boscoboinik, G. Zhou, *Langmuir* **2016**, *32(44)*, 11414–11421; c) Y. Mordekovitz, Y. Shoval, N Froumin, S. Hayun, *Materials* **2020**, *13*, 3195; d) L. Phor, S. Chahal, V. Kumar, *J. Adv. Ceram.* **2020**, *9*, 576-587.

[42] a) A. Hashemi, A. Bahari, *Appl. Phys. A* **2017**, *123(8)*, 535; b) J. Carrasco, D. Lõpez-Durán, Z. Liu, T. Duchoň, J. Evans, S. D. Senanayake, E. J. Crumlin, V. Matolín, J. A. Rodríguez, M. V. Ganduglia-Pirovano, *Angew. Chem. Int. Ed.* **2015**, *54(13)*, 3917–3921; c) J. Lian, P. Liu, C. Jin, Z. Shi, X. Luo, Q. Liu, *Microchimica Acta* **2019**, *186(6)*, 332; d) A. I. Stadnichenko, V. V. Muravev, S. V. Koscheev, V. I. Zaikovskii, H. A. Aleksandrov, K. M. Neyman, A. I. Boronin, *Surf. Sci.* **2019**, *679*, 273–283; e) R. Rios-Escobedo, E. Ortiz-Santos, J. A. Colín-Luna, J. N.; Díaz de León, P. del Angel, J. Escobar, J. A. de los Reyes, *Top. Catal.* **2022**, *65(13–16)*, 1448–1461; f) N. Wang, W. Qian, W. Chu, F. Wei, *Catal. Sci. Technol.* **2016**, *6(10)*, 3594–3605.

[43] T. V. Bui, S. Crossley, D. E. Resasco, in *Chemicals and Fuels from Bio-Based Building Blocks* (Eds: F. Cavani, S. Albonetti, F. Basile, A. Gandini), Wiley-VCH Verlag GmbH & Co. KGaA, Weinheim, Germany, **2016**, Ch.17, pp. 431-494.

[44] a) L. A. de Faria, S. Trasatti, *J. Colloid Interface Sci.* **1994**, *167(2)*, 352–357; b) M. Kosmulski, *J. Colloid Interface Sci.* **2009**, *337(2)*, 439–448; c) A. V. Bandura, S. N. Lvov, *J. Phys. Chem. Ref. Data* **2006**, *35(1)*, 15–30; d) M. Hronec, K. Fulajtárová, T. Soták, *J. Ind. Eng. Chem.* **2014**, *20(2)*, 650–655; e) M. Zeng, *Bull. Korean Chem. Soc.* **2013**, *34(3)*, 953–956.

[45] X. Yang, Y. Mueanngern, Q. A. Baker, L. R. Baker, *Catal. Sci. Technol.* **2016**, *6(18)*, 6824–6835.

[46] X. Li, Z. Tong, S. Zhu, Q. Deng, S. Chen, J. Wang, Z. Zeng, Y. Zhang, J. J. Zou, S. Deng, *J. Catal.* **2022**, *405*, 363–372.

[47] M. Zhou, H. Zhu, L. Niu, G. Xiao, R. Xiao, *Catal. Lett.* **2014**, *144(2)*, 235–241.

[48] Y. Li, X. Guo, D. Liu, X. Mu, X. Chen, Y. Shi, *Catalysts* **2018**, *8 (5)*, 193.

[49] S. Chen, T. T. Qian, L. L. Ling, W. Zhang, B. B. Gong,H. Jiang, *ChemSusChem* **2020**, *13 (20)*, 5507–5515.

[50] W. Tolek, N. Nanthasanti, B. Pongthawornsakun, P. Praserthdam, J. Panpranot, *Sci. Rep.* **2021**, *11 (1)*, 9786.

[51] H. I. Chen and H. Y. Chang, *Ceram. Int.*, 2005, **31 (6)**, 795–802.

[52] J. Shen, J. M. Kobe, Y. Chen and J. A. Dumesic, *Langmuir,* 1994, **10 (10)**, 3902–3908.
[53] M. J. Frisch, G. W. Trucks and H. B. Schlegel. Gaussian 16 (Revision B.01), Gaussian Inc., Wallingford CT, 2017.
[54] S. Grimme, J. Antony, S. Ehrlich and A. Krieg, *J. Chem. Phys.,* 2010, **132 (15)**, 154104.
[55] J. P. Perdew, K. Burke and M. Ernzerhof, *Phys. Rev. Lett.*, 1997, **78 (7)**, 1396.
[56] C. M. M. Rohlfing, P. J. Hay and R. L. Martin, *J. Chem. Phys.*, 1985, **85 (3)**, 1447.
[57] M. Cossi, N. Rega, G. Scalmani and V. Barone, *J. Comput. Chem.*, 2003, **24 (6)**, 669-681.
[58] G. A. Zhurko and D. A. Zhurko, Chemcraft, Version 1.8. https://chemcraftprog.com.

10.1002/cnma.202300158

Table of Contents graphic

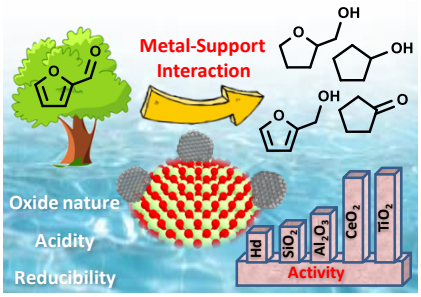

Furfural hydrogenation and surface rearrangements are influenced by the both nature of support and metal-support interaction, which alters the electronic properties of supported nano-Ni particles and surface functionalities of the catalysts. Among different supports used (SiO_2, Al_2O_3, TiO_2, CeO_2, Mg_3AlO_x), the reducible oxides (CeO_2 and TiO_2) display complete conversion of furfural with additional deep-hydrogenated products.

(Loyola College Chennai@lcchennai)